lot of reducing agents, such as organic matter. Moreover, the current XANES study also supports the results of these systems because it suggested that Os was reduced to Os(III) or Os(IV) and that it accumulated in the sediment (Fig. 4). In the presence of organic substances, the variation of redox conditions does not significantly affect the removal behavior of Os because organic matter itself acts as a reducing agent for Os.

In order to investigate the removal of Re and Os under oxic and organic-free conditions, burnt- and oxidized- sediment systems were prepared. In both systems of burnt- and oxidized-sediments (Fig. 8c-1, -2), a significant fraction of Os was also removed from artificial seawater to sediments. These accumulation processes may also be controlled by the reduction of initial Os(VIII). The fact that Os(VIII) species were not adsorbed onto hematite without reduction of Os (VIII) in the short time scale (Fig. 7) and that the reducing potential of Os(VIII)/Os(IV) was 374 mV (at pH 8 and total Os = 10^{-8} M: Brookins, 1988) indicate that initially added Os(VIII) species can be converted to more solid-reactive species in these experimental systems, probably as a result of the reduction of Os(VIII). In the current XANES study, it is confirmed that Os(VIII) was reduced to Os(IV), even in highly oxic air-dried sediments (Eh* = 374 mV).

3.4. Rhenium and Os adsorption onto kaolinite: the effect of humic acid

From the results of the XAFS study and adsorption experiments using Tokyo Bay sediment, it was confirmed that reductive accumulation is relatively significant for both Re and Os in seawater–sediment systems. However, these results cannot provide detailed information on whether or not the reduced Re and Os are inorganically accumulated in marine sediments (adsorption onto minerals or incorporation into authigenic minerals) or are fixed on sediments by complexation with organic matter. In this section, the distribution behaviors of Re and Os between aqueous- and solid-phases were studied in the presence of humic acid (HA) to examine the possibility of their complexation with HA.

3.4.1. Experimental process

Rhenium and/or Os adsorption onto kaolinite in the absence and presence of HA was studied using the multitracer technique. Humic acid was extracted from paddy soil (Tochigi Prefecture, Japan) and was purified (Takahashi et al., 1995, 1998a). Kaolinite, purchased from Wako Chemicals Ltd., had a surface area of 7.5×10^2 m^2/g (Takahashi et al., 1998b). Weighed kaolinite (10 mg) was mixed with 5 ml of HA solution (30 mg/dm^3) or Milli-Q water in a polystyrene beaker. The ionic strength of the solution was adjusted to 0.020 M with NaCl, and its pH value was adjusted with a small amount of NaOH or HCl solution. In the metal–kaolinite–HA system, two types of experiments were conducted to check the effect of the order of injections of multitracer and HA: one type of experiment involves addition of the multitracer followed by HA after shaking for 5 days, while the other involves addition of HA followed by the multitracer. After shaking the solution

for 10 days, the kaolinite was filtered out using a 0.45 μm membrane filter to recover the aqueous phase. The absorbance of the filtrate at 420 nm was compared with that of an initial HA solution (30 mg/dm^3) at a pH and ionic strength identical to each sample in order to determine the dissolved fraction of HA. One may think that seawater would make a better experimental aqueous phase for this study, since HA is pre-equilibrated with seawater in the natural marine environment. However, HA is readily coagulated in high ionic strength solutions such as seawater (=0.7 M), and this situation is not good for observation of competition between adsorption onto kaolinite and humate formation in the aqueous phase; competition is needed in this experimental system to semi-quantitatively examine the effect of humate formation. Thus, a 0.020 M NaCl solution was applied in this experiment.

3.4.2. Adsorption in the absence and presence of humic acid

The pH dependence of adsorption of Re and Os on kaolinite in the absence and presence of HA accompanied by the pH dependence of HA distribution is shown in Fig. 9. Since HA is subjected to either precipitation or adsorption under acidic conditions, the dissolved fraction of HA was small, especially below pH 2. As the pH level increases,

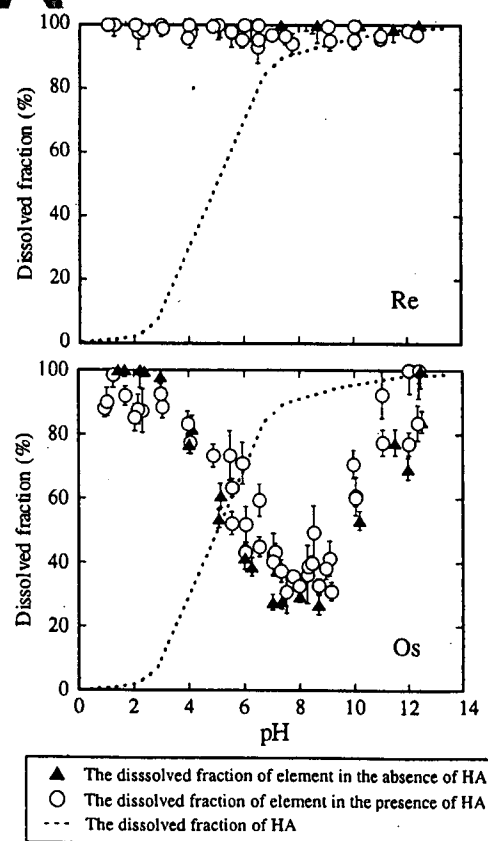|	
▲	The disssolved fraction of element in the absence of HA
O	The dissolved fraction of element in the presence of HA
- - -	The dissolved fraction of HA

Fig. 9. The pH dependence of the dissolved fractions of Re and Os in contact with kaolinite in the absence and presence of HA. Kaolinite 10 mg; water 5.0 ml; initial concentration of HA: 30 mg/dm^3. The ionic strength was adjusted to 0.020 M with NaCl.

the HA molecule becomes negatively charged due to the deprotonation of the ligands, thereby promoting its dissolution. Under alkaline conditions, most of the HA was dissolved due to enhancement of the repulsion between dissociated HA and negatively charged kaolinite.

The adsorption of Re on kaolinite was not observed in the absence or presence of HA (Fig. 9). Irrespective of the order of injections of the multitracer and HA, the addition of HA did not influence the distribution of Re, suggesting that complexation with HA is not important for Re, at least not for ReO_4^-.

In both the binary (Os + kaolinite) and ternary (Os + kaolinite + HA) systems, the dissolved fraction of Os was minimal at neutral pH. These distribution patterns can be explained by the high reactivity of reduced Os, probably Os(III) and/or Os(IV) hydrolyzed species, with kaolinite surface around neutral pH (Fig. 9). Since the redox potential of the Os(VIII)/Os(IV) couple is high (e.g., 374 mV at pH 8 and Os = 10^{-8} M: Brookins, 1988), Os(VIII) can be reduced to Os(IV) in water under ambient air condition. Under neutral to alkaline pH conditions (5 < pH < 10), the dissolved fraction of Os in the ternary system is slightly but systematically larger than that in the binary system. The binary and ternary system patterns intersect with each other at around pH 4. Under acidic conditions (pH < 3), although the dissolved fractions of both systems are close to 100%, the dissolved fraction of Os in the ternary system is slightly lower than that in the binary system. This result implies that a small amount of Os was fixed on kaolinite due to its complexation with HA adsorbed on the solid surface. Similarly, the dissolved fraction of HA binding to Os leads to an increase in the dissolved fraction of Os between pH 5 and 10 in the ternary system. If humate complex is dominant species both in the aqueous phase and on kaolinite, the distribution of the ion should be identical to that of HA (Takahashi et al., 1999). However, the dissolved fraction of Os was not identical to that of HA in this region, showing that there are other Os species adsorbed on the kaolinite and dissolved in the aqueous phase. It has been empirically confirmed that Os (and/or Re) is considerably enriched in organic-rich sediment, which is well correlated with total organic carbon (Ravizza et al., 1991). However, the result of this experiment is inconsistent with these observations probably because Os enrichment requires the development of reducing conditions with the presence of organic matter.

3.5. Sequential extraction

The sediment that is rich in organic matter can be a sink of Re and Os under reducing marine environments (Ravizza et al., 1991). In addition, it was reported that a portion of Os dissolved by black shale weathering can be incorporated in ferromanganese oxides (Pierson-Wickmann et al., 2002). In order to identify the host phase of Re and Os in the sediment, sequential extraction experiments (Tessier et al., 1979; Koschinsky and Halbach, 1995) were performed for the reducing sediments (untreated Tokyo Bay sediment) containing multitracer in the adsorption experiments.

3.5.1. Experimental process

The leaching protocols followed those described in the studies of Tessier et al. (1979), Koschinsky and Halbach (1995) (see Appendix C for the details). The results show the six fractions of Re and Os including the aqueous phase in the system: (F1) seawater, (F2) exchangeable ion, (F3) carbonate, (F4) ferromanganese oxide, (F5) organic matter, and (F6) insoluble residue. In each extraction step, following the first separation of leaching solution (or artificial seawater), the residual sediment was washed with a few milliliter of leaching solution (or artificial seawater). The rinse solution was recovered by centrifugation and was mixed with the former. Gamma-ray analyses were performed on each fraction where the volume of each sample was constant at 25 ml, except for the insoluble residue (F6). The gamma-ray spectrum of the insoluble residue was then measured for the solid sample. The spectrum peak area for the residue was corrected by means of the correction factors obtained by comparing the detection efficiencies in the cases of solution (25 ml) and residual solid.

3.5.2. Results of sequential extraction

The sequential extraction results (Fig. 10) show the distribution of Re in the whole system in sorption experiments among the following phases: 70% in seawater (F1), 15% in exchangeable ion (F2), 2% in carbonate (F3), 5% in Fe–Mn oxide (F4), and 8% in organic matter (F5). The Re fractions belonging to F2–F5 may be in reduced forms, and based on thermodynamic calculations, it is thought that ReO_4^- reduction can occur under experimental conditions (pH 7.9, Eh = −191 mV). However, the results of sequential extraction also suggest that Re mainly exists as a dissolved species despite being partly incorporated in the reducing sediments.

Osmium was mainly found in the three fractions of organic matter (F5): ferromanganese oxides (F4), and seawater
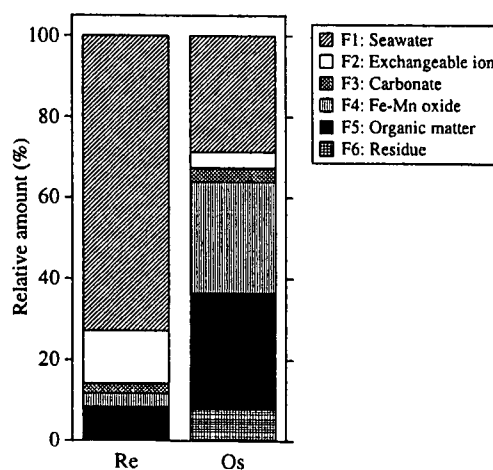

Fig. 10. Relative amount of Re and Os in six fractions (F1–F6) in the sequential extraction. The redox condition of the seawater-sediment system is pH 7.9 and Eh −191 mV. For the fractions recovered over 20%, RSD (%) calculated from repeated experiments (n = 3) was less than 20% of each value.

Legend:
- F1: Seawater
- F2: Exchangeable ion
- F3: Carbonate
- F4: Fe-Mn oxide
- F5: Organic matter
- F6: Residue

(F1). This result suggests that Os was incorporated in the reducing sediment as more than one chemical species. This suggestion is supported by the XANES study, which showed that the predominant Os species in marine sediments were Os(IV) and Os(III). Thirty percent and 10% of the total Os was found in ferromanganese oxides and the residual phase, respectively. Osmium incorporated in these phases may correspond to the hydrolyzed Os species at lower valences (III or IV), favoring sorption to mineral surfaces due to its large ionic potential. On the other hand, 30% of Os was incorporated in the organic matter fraction. This result implies the possibility that a fraction of Os can be complexed with organic matter. Although further study is needed to confirm the preference of Os as organic complexes, the distribution of Os in the organic matter fraction is supported by the adsorption study in the presence of HA (Section 3.4), where Os can form HA complexes to some degree.

It is possible that the re-oxidation of redox sensitive elements during each extraction step can occur in the sequential extraction experiments. Although the possibility of re-oxidation cannot be denied in the current experimental system, re-oxidation does not significantly affect the results, because (i) a large amount of Re is still retained as the Re(VII) species dissolved in artificial seawater in anoxic seawater–sediment systems (Figs. 3, 8-a, and 10), and (ii) if re-oxidation of Os occurred, the fractions of the exchangeable ion and carbonate should be larger. However, the fractions of ferromanganese oxides and organic matter still account for a large fraction of total Os (=collectively 60%). Hence, the results of the sequential extraction experiments in this study may be acceptable.

4. DISCUSSION

In this chapter, the geochemical behaviors of Re and Os in a marine environment are discussed by combining the results of the two types of experiments, which are then compared with the results of the behavior of Re and Os in a natural seawater–sediment system reported in previous studies. The understanding of Re/Os fractionation in various redox marine environments is also extended.

4.1. The geochemical behavior of Re in a seawater–sediment system

The conservative behavior of Re in a natural marine environment was reported by Anbar et al. (1992) and Colodner et al. (1993). They revealed that the Re concentration in seawater is constant throughout the water column, and that dissolved Re cannot be adsorbed onto suspended particles. On the other hand, many studies dealing with marine sediments have also pointed out that Re is highly enriched in organic-rich reducing sediments (Ravizza et al., 1991; Crusius et al., 1996; Cohen et al., 1999; Selby and Creaser, 2003). These reports are well consistent with the current laboratory results. In the current study's oxic experimental systems, Re showed conservative behavior: for instance, (i) the adsorption of ReO_4^- on various minerals was not observed, (ii) ReO_4^- did not

interact with humic acid, and (iii) the ReO_4^- form was kept in the seawater–sediment system for 2 weeks. On the other hand, Re was enriched in organic-rich reducing sediment along with the development of a reducing condition in the adsorption study using untreated Tokyo Bay sediment and sequential extraction (Figs. 8a and 10). These results obviously suggest that Re removal can be controlled by chemical reduction. The XANES study robustly supports the reductive removal of Re as it suggests that Re incorporated in the reducing sediment within 2 weeks was partly reduced to lower oxidation states (Fig. 2). The Re XANES simulation with ReO_4^- and ReO_2 showed that the contributions to total Re in the reducing sediment from ReO_4^- and ReO_2 are 73% and 27%, respectively (Fig. 2). Although complete ReO_4^- reduction was not attained during the 2-week time frame [reducing potential of experimental system: $Eh^* = -273$ mV (or $Eh = -108$ mV at pH 5.2); reducing potential of ReO_4^-/ReO_2 couple: $Eh = -235$ mV at pH 8 and total $Re = 10^{-6}$ M: Brookins, 1988], this speciation is likely to be consistent with Re in the natural marine environment. Colodner et al. (1993) reported that dissolved Re can exist in the porewater of both oxic and reducing sediments. The fact that the distribution behavior and speciation of Re yielded by the multitracer and XANES studies are similar to those observed in nature indicates that ReO_4^- is a predominant Re species in reducing seawater–sediment system, even under sulfidic conditions. It can be thought that ReO_4^- reduction proceeds very slowly, even if the reducing potential of the experimental system reaches that of the ReO_4^-/ReO_2 couple. At the least, complete reduction was not attained within the given 2-week laboratory time scale. The slow reduction mechanism of Re was previously proposed by Crusius and Thomson (2000), Sundby et al. (2004). Based on the sediment-core study, they explained that the kinetics of Re accumulation can be controlled by a proposed multistep reduction mechanism in which, to a greater extent, longer times are required for the accumulation of Re in the sediment. The possible slow reduction mechanism in our experimental system can be confirmed by comparing the oxidation states of Re and S. Based on the reducing potentials of Re and S and the current S XANES study, (i) the reducing potential of the ReO_4^-/ReO_2 couple (-235 mV at pH 8 and total $Re = 10^{-6}$ M: Brookins, 1988) is higher than that of sulfate reduction (the reducing potential of SO_4^{2-}/HS^- is -305 mV at pH 8 and total dissolved S concentration is assumed to be 10^{-3} M: Brookins, 1988) and (ii) the current S XANES study suggests that the main S species in reducing sediments (UDS-G series) is sulfide (=98%). The fact that Re(IV) was not formed under the Eh condition where sulfide can be formed strongly suggests that the reduction of ReO_4^- to Re(IV) is slow.

Although the resistance of ReO_4^- to chemical reduction, the low reactivity of hydrated ReO_4^- ion with the oxide surface and the binding site of organic substances all cause the conservative behavior of Re in the seawater–sediment system, it was experimentally revealed in the current study that it is primarily chemical reduction that affects the accumulation of Re in the marine environment.

4.2. The geochemical behavior of Os in a seawater–sediment system

There are only a few previous studies which discussed the removal mechanism of Os in chemical terms (Koide et al., 1991; Woodhouse et al., 1999; Levasseur et al., 2000). All of these studies described the geochemical behavior of Os based on analyses of natural sediments or seawater with thermodynamic calculations. Here, the removal mechanism of Os is discussed by combining the current experimental results and the knowledge gained from previous reports.

Osmium is also known to be enriched with organic-rich reducing sediment (Ravizza et al., 1991; Cohen et al., 1999; Selby and Creaser, 2003). This empirical fact together with the thermodynamically expected Os dissolved species, Os(VIII) oxyanion, led Os geochemists to suggest that Os accumulates through reductive reaction (Woodhouse et al., 1999; Dalai et al., 2005). Based on seawater analyses, Levasseur et al. (1998) proposed that the geochemical behavior of Os can be controlled by inert organic matter, and that it can be conservative in marine environments. The current laboratory experiments are consistent with these previous suggestions. For instance, Os gradually and significantly accumulated into organic-rich sediments along with the development of a reducing condition (Figs. 8a, b and 10). This result indicates that Os can be incorporated in the sediments as a result of reduction from Os(VIII)-dissolved species. The reductive accumulation of Os is confirmed by the current XANES study (see Section 2.2.2 and Fig. 4). In addition, the distribution study using HA suggests that the aqueous behavior of Os was partly affected by HA. This distribution study also implies that there was another Os species in this experimental system, likely the Os hydrolysis species. In sequential extraction, it can also be seen that there are more than one Os species in seawater–sediment systems: one is in the organic-matter phase, and the other is in the Fe–Mn oxide or residual phase. The inference that there are more than one Os species in the seawater–sediment system is robustly confirmed by the Os XANES study. The results of XANES reveal that the Os incorporated in the reducing sediment was mainly in a trivalent state, and Os in the oxic (air-dried) sediment was mainly in a tetravalent state (Fig. 4). These results clearly suggest that the primary and secondary Os species in marine sediments are Os(III) and Os(IV), respectively, and that the Os(III)/Os(IV) ratio can change along with the variation of redox conditions.

If Os is dissolved in seawater as the Os(VIII) oxyanion, a reductive reaction is important for Os removal in seawater–sediment systems. In this case, the reducing agent may not be restricted to organic matter in seawater because Os(VIII) has a highly oxidizing property. For example, Mn(II) or Fe(II) may also play the role of a reducing agent for Os(VIII) in a natural oxic marine environment. In the current experimental systems, Os was readily removed from the artificial seawater to sediments even in the absence of organic matter (Fig. 8c-1, -2). The Os XANES result suggests that Os was reduced from the initial Os(VIII) to Os(IV) species even in oxic sediments (ADS series: Eh* = 357 and

374 mV), and the results can be reasonably explained by previous thermodynamic estimations (Brookins, 1988). On the other hand, in the case where $OsCl_6^{2-}$ is assumed to be the Os dissolved species in seawater, initially coordinated Cl can be replaced by O through hydrolysis during the removal process, as confirmed by the EXAFS data (Figs. 5 and 6, and Table 2). Reduced Os from Os(VIII) to Os(IV) and/or initially dissolved $OsCl_6^{2-}$ is readily subjected to hydrolysis and adsorbed onto the mineral surfaces, or it may accumulate with the precipitation of authigenic minerals under relatively oxic conditions (e.g., Figs. 8c-1, -2, and 9). In nature, it has been reported that Os can be enriched in authigenic sediments (minerals), such as ferromanganese oxides, in oxic marine environments (Palmer et al., 1988; Koide et al., 1991; McDaniel et al., 2004). This accumulation process can be explained by the reactivity of the hydrolyzed metal (III or IV) ion with the surface of solids, as described in the results of the sequential extraction.

Following first burial as Os(IV), Os(IV) can be reduced further to Os(III) along with the development of reducing conditions. During this step, organic matter can act as a principal reducing agent and as a carrier for Os, probably by complexation. The possibility of the formation of Os–organic complex was partly supported by the results of the distribution study using HA and sequential extraction. The current Os EXAFS study also provides supportive information for the speciation of Os in the reducing sediments. The EXAFS results suggest that the O atom is the first neighboring atom of Os in the reducing sediment and that the Os–O bond length is approximately 2.00 Å. If Os is actually bound by organic ligands in the reducing sediment, the O atom at the deprotonated ligand of organic matter such as carboxylate can be a main binding site of Os. Moreover, a slightly and systematically longer Os–O bond length (about 2.00 Å) than that of the available Os(IV) oxide reference material (about 1.96 Å) seems to indicate the possibility of an Os(III)–organic complex (see Section 2.2.3).

Osmium can be in various oxidation states in natural marine environments because of its redox sensitivity. In more detail, it is confirmed that the main oxidation states of Os in the seawater–sediment system are tri- and tetra-valent. These Os ions can be readily subjected to hydrolysis and adsorbed onto solid surfaces, and partly interact with organic matter as well. The geochemical behavior of Os is controlled by many processes (described above), and it can be readily incorporated onto marine sediment under various redox environments.

4.3. Rhenium and Os fractionation

Many studies have reported that both Re and Os are enriched in reducing sediment that contains a high proportion of organic carbon (Ravizza et al., 1991; Cohen et al., 1999; Selby and Creaser, 2003; McDaniel et al., 2004). Based on the current experiments, it is clear that the geochemical behaviors of Re and Os in the seawater–sediment system are not similar, although both elements tend to be enriched in organic-rich reducing sediments. Large fractionation between Re and Os likely occurs during removal from seawater

to sediment. In this chapter, the $^{187}Re/^{188}Os$ ratio of the reducing sediment in the adsorption experiment (Fig. 8a) is calculated, and the fractionation between Re and Os during their removal is discussed by comparing the calculated $^{187}Re/^{188}Os$·ratio with those of the geological materials. As a first step, the distribution coefficients (K) of Re and Os are calculated using the data obtained from the adsorption experiment (Fig. 8a, at 168 h). The equation of K is described below:

$$K = \frac{(100 - R)/W_{sediment}}{R/W_{artificial\ seawater}} \quad (2)$$

where $R(\%)$ is the dissolved fraction of the element in artificial seawater at the end of the experiments, and W is the weight of artificial seawater or sediments. The model $^{187}Re/^{188}Os$ in the sediment, $(^{187}Re/^{188}Os)_{sed}$, is calculated below:

$$\left(\frac{^{187}Re}{^{188}Os}\right)_{sed} = \left\{\frac{(C_{Re} \times F_{^{187}Re}/N_{^{187}Re}) \times A}{(C_{Os} \times F_{^{188}Os}/N_{^{188}Os}) \times A}\right\}^{*} \times \frac{K_{Re}}{K_{Os}} \quad (3)$$

where C is the concentration of Re or Os in natural seawater, F is the isotopic abundance of ^{187}Re or ^{188}Os in natural seawater, N is the atomic mass of ^{187}Re or ^{188}Os, A is Avogadro's number, and K is the distribution coefficient of Re or Os. In this equation, the term in larger brackets (*) denotes the isotopic abundance ratio between ^{187}Re and ^{188}Os in natural seawater. In practice, a previously reported $^{187}Re/^{188}Os$ ratio for natural seawater (=4270, Peucker-Ehrenbrink and Ravizza, 2001) was applied in this calculation.

Only the $^{187}Re/^{188}Os$ ratio for untreated sediment can be calculated because Re was not removed to sediment except in the case of untreated sediment in the current adsorption experiment (Fig. 8). When the detrital fraction of Re or Os is not considered, the $^{187}Re/^{188}Os$ ratio for reducing sediment (Eh* = −136 mV, measured Eh = −48 mV at pH

6.5) derived from Re and Os removal from artificial seawater was estimated to be approximately 120, as shown by ▲ in Fig. 11. It was reported that $^{187}Re/^{188}Os$ variations in sediment rich in organic matter ranged from one hundred to several thousands (Ravizza et al., 1991; Cohen et al., 1999; Selby and Creaser, 2003). The calculated $^{187}Re/^{188}Os$ for untreated sediment falls within the $^{187}Re/^{188}Os$ range reported in previous studies, and is higher than that of continental detritus such as loess (10–50: Hattori et al., 2003), but is lower, by about one order of magnitude, than that of average seawater (4270: Peucker-Ehrenbrink and Ravizza, 2001). This fact confirms that a large amount of Re and Os in sediments is derived from seawater in anoxic marine environments, as well as large fractionations between Re and Os occurring during their removal from seawater to sediments. It is known that natural Mn nodules (and other authigenic minerals) have an extremely low $^{187}Re/^{188}Os$ (~1: McDaniel et al., 2004) ratio under oxic marine environments, compared with seawater and/or continental detritus. Consequently, the $^{187}Os/^{188}Os$ ratio is roughly equal to that for average seawater. However, the model $^{187}Re/^{188}Os$ ratio for the oxic sediment (Eh* = 120–470 mV) cannot be calculated because no Re removal was observed in these experiments. The $^{187}Re/^{188}Os$ ratio observed in natural oxic sediments or authigenic minerals can be explained by the current experimental results. That is, Re cannot be incorporated into solid phases under oxic conditions (most of Re in these sediments would be derived from detritus). On the other hand, Os can be readily removed to solid phases even under oxic conditions. Accordingly, the $^{187}Re/^{188}Os$ ratio of oxic sediments (and authigenic minerals) can be lower as the contribution of authigenic phases becomes larger in the sediment.

The current study's results confirm that the $^{187}Re/^{188}Os$ variations of marine sediments and sedimentary rocks under various redox conditions are controlled by whether Re can be incorporated into the sediment. Under a reducing environment as described above, Re can be incorporated to larger degree, which induces a high $^{187}Re/^{188}Os$ ratio in the sediment (Fig. 11). The higher $^{187}Re/^{188}Os$ ratio causes larger growth of the $^{187}Os/^{188}Os$ ratio in natural rocks. Hence, organic-rich sedimentary rocks, such as black shales, can be targeted for Re–Os dating. In contrast, since only Os can be removed under an oxic environment, and given that Re in these sediments (and authigenic minerals) is only derived from detritus, the $^{187}Re/^{188}Os$ of authigenic materials such as ferromanganese oxide is lower than that of continental detritus (Fig. 11). The Os isotope system of authigenic materials that occurs in an oxic marine environment can be used as a paleo-marine environmental tracer because the growth of $^{187}Os/^{188}Os$ is not prominent due to the lower $^{187}Re/^{188}Os$ ratio. This interpretation of $^{187}Re/^{188}Os$ variation in various marine environments should be kept in mind during the discussion of Re–Os isotope systems in various sediments and sedimentary rocks.
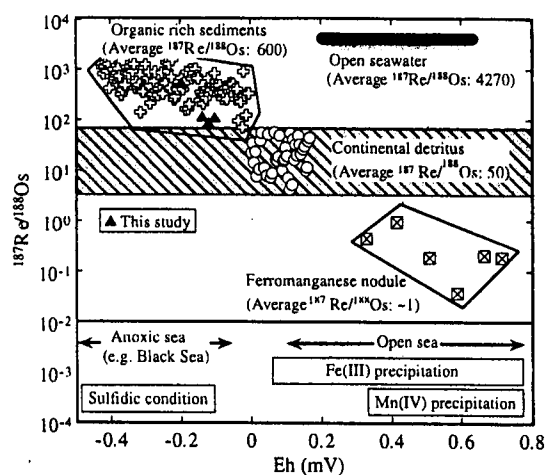
Fig. 11. Relationship between the redox condition in seawater and possible $^{187}Re/^{188}Os$ ratios in the sediments found in each environment. The estimated $^{187}Re/^{188}Os$ ratios based on our partitioning study were also plotted. The redox potential (or marine redox conditions) of each natural sample is assumed based on Brookins (1988), Langmuir (1997).

5. SUMMARY AND CONCLUSIONS

In this paper, the removal behaviors of Re and Os in a seawater–sediment system and Re/Os fractionation during

removal were studied by performing laboratory experiments using a multitracer technique and XAFS spectroscopy. A schematic diagram summarizing the accumulation processes and possible chemical species of Re and Os in the marine environment is shown in Fig. 12. The conclusions of this study are summarized as follows:

(a) The XAFS study revealed that Os incorporated in reducing sediments was mainly trivalent, and its first neighboring atom was O (the bond length is about 1.984–2.017 Å). Moreover, Os removed to dried sediments under oxic conditions was mainly in a tetravalent state. It is suggested that Os is first incorporated into the oxic sediments as Os(IV), mainly as the Os(IV) hydrolyzed species. Subsequently, Os(IV) can be reduced to Os(III) in organic-rich sediments with the development of a reducing environment. These results confirmed that Os(III) and Os(IV) coexist in seawater–sediment systems along with the variation of redox conditions.

(b) The ionic forms of Re and Os in artificial seawater were confirmed to be negatively charged. The current XANES study showed that Re in seawater can exist as ReO_4^- under various redox conditions, and that Os in water extracted from activated carbon is an octavalent species. If Os maintains its octavalent state in seawater during the contact time (30 min), its dissolved species may be anionic hydrolyzed species such as $HOsO_5^-$ or $H_3OsO_6^-$. This Os speciation

seems to be correct in the highly oxic open ocean, but our study suggests that Os(IV) hydrolyzed species is more important in a seawater–sediment system.

(c) Rhenium and Os can be removed from artificial seawater to sediments with the development of reducing conditions, confirming that reductive removal is an important process for Re and Os. The removal of Os from the seawater to burnt sediment and organic-free sediment under oxic conditions was also observed, while Re was not removed from the seawater to the sediments under the same conditions. The removal process of Os seems to be controlled by several factors, such as reduction, hydrolysis, and inorganic complexation.

(d) The results of the adsorption experiment in the absence and presence of humic acid suggest that complexation with humic acid influences the distribution behavior of Os to some degree. Osmium also showed high affinity to an oxide surface, even in the presence of humic acid, suggesting the existence of hydrolyzed insoluble Os species.

(e) The sequential extraction showed that about 80% of Re remained in the seawater fraction after a 2-week incubation period despite a substantial Eh decrease. The XANES spectrum for Re in reducing sediment suggested that most Re existed as ReO_4^- in the reducing sediments. The XANES results also suggest that the reductive reaction of Re(VII) proceeds very slowly, probably due to its slow kinetics. Complete ReO_4^- reduction was not attained during the 2-week time scale in the laboratory experiments. Sequential

Fig. 12. Schematic diagram for the removal mechanism, possible chemical species of Re and Os, and variations of the $^{187}Re/^{188}Os$ ratio in geological samples in marine environments. The $^{187}Re/^{188}Os$ ratios of continental loess, ferromanganese oxides, and black shale followed the reports of Hattori et al. (2003), McDaniel et al. (2004), Selby and Creaser (2003), McDaniel et al. (2004), respectively.

extraction suggested that Os was distributed into three fractions, namely, seawater, Fe–Mn oxides, and organic matter. These results further suggest that Os assumes more than one species in a seawater–sediment system, which was also supported by the XAFS study. Osmium in the ferromanganese oxide and residual phases may be a hydrolyzed Os(III or IV) species favoring mineral surfaces due to its high ionic potential, while Os in the organic-phase may be Os(III) complexed with organic matter.

(f) Although Re is removed to sediments only under highly reducing condition in our experiments, the slow kinetics of Re reduction can inhibit the observation of Re removal under less reducing condition within the timescales of the experiments. Actually, Re can be removed under mildly reducing condition in natural marine environments (Crusius et al., 1996; Morford et al., 2007). Hence, we here conclude that reducing condition is needed for the removal of Re to sediments, while Os can be removed even under oxic condition as shown in our experiments. Thus, a high $^{187}Re/^{188}Os$ ratio can occur in reducing sediments, such as black shales. The high $^{187}Re/^{188}Os$ ratio makes black shales suitable for Re–Os dating due to the larger growth of $^{187}Re/^{188}Os$. In contrast, authigenic sediments (and minerals) under oxic environments can only enrich Os, which causes a much lower $^{187}Re/^{188}Os$ ratio than that of seawater. The osmium isotope system of these materials can be used as a paleo-marine environmental tracer because the $^{187}Os/^{188}Os$ ratio cannot grow significantly due to its extremely low $^{187}Re/^{188}Os$ ratio.

APPENDIX A. ARTIFICIAL SEAWATER AND TOKYO BAY SEDIMENT

The chemical composition of artificial seawater followed that in the study of Tsunogai and Noriki (1983); Milli-Q water: 1000 g, NaCl: 23.5 g, $MgCl_2 \cdot 6H_2O$: 10.6 g, Na_2SO_4: 3.98 g, $CaCl_2 \cdot 2H_2O$: 1.48 g, $NaHCO_3$: 0.19 g.

The chemical composition determined by XRF for the Tokyo Bay sediment is as follows: SiO_2: 50.4 wt%; TiO_2:

0.6 wt%; Al_2O_3: 14.3 wt%; Fe_2O_3: 5.7 wt%; MnO: 0.09 wt/%; MgO: 2.6 wt%; CaO: 2.9 wt%; Na_2O: 3.99 wt%; K_2O: 1.6 wt%; P_2O_5: 0.12 wt%.

APPENDIX B. XAFS MEASUREMENT AND ANALYSIS

Rhenium L_{III}-edge XAFS spectra were measured at the beamline 12C in KEK-PF (Tsukuba, Japan) where a Si (111) double-crystal monochromator and a bent cylindrical mirror were employed to obtain monochromatic X-ray. Osmium L_{III}-edge XAFS spectra were obtained at the beamline BL01B1 in SPring-8 (Hyogo, Japan) equipped with a Si (111) double-crystal monochromator using two mirrors. The measurements were carried out at room temperature. The energy calibration was conducted for Re and Os L_{III}-edges with ReO_2 and $OsCl_3$, respectively. In order to obtain fluorescent XAFS spectra for the sediment samples, a 19-element Ge solid state detector (SSD) was employed and Al foil was placed between the sample and the detector to reduce the entry of X-ray fluorescence in SSD from major elements such as Fe and Mn in sediments. By taking repeated scans for most of the samples, a possible change of XAFS spectra due to the alteration of Os and Re species during XAFS measurements was checked. As a result, it was found that no appreciable change in the XAFS spectra was observed, and the repeated scans were averaged to obtain each XAFS spectrum.

In the case of fluorescence XAFS measurements by SSD, dead time corrections were made for the SSD counting. XANES and EXAFS analyses were performed using REX2000 Ver. 2.3 (Rigaku Co.). For the XANES data measured in fluorescence mode, the background absorption was subtracted using a linear function estimated from pre-edge region. On the other hand, the Victoreen equation was applied for the calculation of background absorption of the spectra obtained by the transmission mode. Following the subtraction of background, the spectra were normalized to absorption at the post-edge region. For the EXAFS region, after background correction and normalization, the smooth L_{III}-edge absorption of the free Os atom (μ_0) was removed using a spline curve. EXAFS function $\chi(k)$ was extracted from the XAFS spectrum by transforming incoming X-ray energy units (keV) to photo-electron wave number (Å^{-1}). Fourier transformation of k^3-weighted $\chi(k)$ function from k-space (Å^{-1}) to R-space (Å) was performed to obtain a radial structural function (RSF) in the k (Å^{-1}) range $3.25 < k < 7.05$ for all the Os samples. The k range used for the fourier transformation was determined based on the available k range for sediment samples. A Fourier inverse transformation was performed on the first shell of the RSF. The theoretical EXAFS function was fitted to an inversed k^3-weighted $\chi(k)$ function using parameters provided by FEFF7.0 (Zavinsky et al., 1995; Ankudinov and Rher, 1997). The EXAFS analysis provides the coordination number (N), the interatomic distance (R), the energy offset (dE), and the Debye–Waller factor (DW) for the first shell in this study. Following Stern (1993), the maximum number of parameters for curve fittings (N_{free}) were calculated ($N_{free} = 4$). Considering the coordination number of

Os standard materials ($OsCl_6^{2-}$ $OsO_2 \cdot nH_2O$, and OsS_2), the coordination number of Os in sediment was fixed at 6. Assessing the quality of each fitting, the R-factor, showing the difference between experimental and theoretical $\chi(k)$ functions, was utilized (Sakakibara et al., 2005).

APPENDIX C. PROTOCOLS OF SEQUENTIAL EXTRACTION

The protocols of sequential extraction basically followed those described in the studies of Tessier et al. (1979) and Koschinsky and Halbach (1995).

(1) Upon adsorption of the multitracer, the polystyrene beaker was centrifuged, and the seawater (F1) was recovered as much as possible. The residual sediment was air-dried and disaggregated in the beaker.

(2) An aliquot of sediment (0.8 g) was treated with 8 ml of 1.0 M sodium acetate at pH 8.0. The sample was shaken for 1 h at room temperature. The aqueous phase was separated by centrifugation. This step extracts easily exchangeable ions (F2).

(3) The residue from (2) was mixed with 8 ml of 1.0 M sodium acetate at pH 5.0 and was shaken for 10 h at room temperature. This step leaches the elements bound to the carbonate (F3).

(4) The residue from (3) was treated with 20 ml of 0.20 M ammonium oxalate (pH 3.5) and was shaken for 24 h at room temperature. This step extracts elements bound to the ferromanganese oxides (F4).

(5) The residue from (4) was mixed with 3 ml of 0.020 M HNO_3 and 5 ml of 30 wt% H_2O_2 (pH 2.0, adjusted with HNO_3), and was shaken at 60 °C until the vigorous reaction was terminated. Thirty wt% H_2O_2 (5 ml) was reloaded and shaken in the same way. The aqueous phase was recovered by centrifugation. After that, 5 ml of 3.2 M ammonium acetate (pH 2.0) was introduced into the residue and it was shaken for 1 h at room temperature. The liquid phase was separated by centrifugation and was mixed with the former. This step extracts elements bound to the organic matter (F5).

(6) The residue (F6) from (5) was air-dried.

REFERENCES

Ambe S., Chen S. Y., Ohkubo Y., Kobayashi Y., Maeda H., Iwamoto M., Yanokura M., Takematsu N., and Ambe F. (1995) "Multitracer" a new tracer technique—its principle, features, and application. *J. Radioanal. Nucl. Chem.* **195**, 297–303.

Ambe F. (1996) The Multitracer,. Its Application to Chemistry, Biochemistry and Biology, RIKEN review, vol. 13.

Anbar A. D., Creaser R. A., Papanastassiou D. A., and Wasserburg G. J. (1992) Rhenium in seawater: confirmation of generally conservative behavior. *Geochim. Cosmochim. Acta* **56**, 4099–4103.

Ankudinov A. L., and Rher J. J. (1997) Relativistic calculations of spin-dependent X-ray absorption spectra. *Phys. Rev. B* **56**, 1712–1716.

Baes C. F., Jr., and Mesmer R. E. (1986) *The Hydrolysis of Cations*. Krieger Rub. Com., Florida.

Bohn H. L. (1971) Redox potentials. *Soil Sci.* **112**, 39–45.

Boman C. E. (1970) Precision determination of the crystal structure of osmium dioxide. *Acta Chem. Scand.* **24**, 123–128.

Brookins D. G. (1988) *Eh–pH Diagrams for Geochemistry*. Springer, Berlin.

Cohen A. S., Coe A. L., Bartlett J. M., and Hawkesworth C. J. (1999) Precise Re–Os ages of organic-rich mudrocks and Os isotope composition of Jurassic seawater. *Earth Planet. Sci. Lett.* **167**, 159–173.

Cotton F. A., and Rice C. E. (1977) Structure of the high-temperature form of osmium(IV) chloride. *Inorg. Chem.* **16**, 1865–1867.

Cotton F. A., and Wilkinson G. (1980) *Advanced Inorganic Chemistry*, fourth ed. Wiley, New York.

Colodner D., Sachs J., Ravizza G., Turekian K. K., Edmond J., and Boyle E. (1993) The geochemical cycle of rhenium: a reconnaissance. *Earth Planet. Sci. Lett.* **117**, 205–221.

Colodner D., Edmond J., and Boyle E. (1995) Rhenium in Black Sea: comparison with molybdenum and uranium. *Earth Planet. Sci. Lett.* **131**, 1–15.

Crusius J., Calvert S., Pederson T. F., and Sage D. (1996) Rhenium and molybdenum enrichments in sediments as a indicators of oxic, suboxic and anoxic conditions of deposition. *Earth Planet. Sci. Lett.* **145**, 65–79.

Crusius J., and Thomson J. (2000) Comparative behavior of authigenic Re, U, and Mo during reoxidation and subsequent long-term burial in marine sediments. *Geochim. Cosmochim. Acta* **64**, 2233–2242.

Dalai T. K., Suzuki K., Minagawa M., and Nozaki Y. (2005) Variations in seawater osmium isotope composition since the last glacial maximum: A case study from Japan Sea. *Chem. Geol.* **220**, 303–314.

Hattori Y., Suzuki K., Honda M., and Shimizu H. (2003) Re–Os isotope systematics of the Taklimakan Desert sands, moraines and river sediments around the Taklimakan Desert, and of Tibetan soils. *Geochim. Cosmochim. Acta* **67**, 1195–1205.

Hayashi K., Serikawa D., Maeda N., Okamoto A., and Ikeuchi T. (2000) Microwave absorption materials - IV Preparation of the mixed layer structure phases, $Re_x Ta_{1-x} S_2$ and $Os_x Ta_{1-x} S_2$, and some electrical and magnetic properties. *J. Eur. Ceram. Soc.* **20**, 2735–2742.

Iida A. (2000) Instrumentation for μ-XRF at synchrotron sources. In *Microscopic X-ray Fluorescence Analysis*, (eds. K.H.A. Janssens, F.C.V. Adams and A. Rindby), p. 142. Wiley, Chichester.

Koide M., Goldberg E. D., Niemeyer S., Gerlach D., Hodge V., Bertine K. K., and Padova A. (1991) Osmium in marine sediments. *Geochim. Cosmochim. Acta* **55**, 1641–1648.

Koschinsky A., and Halbach P. (1995) Sequential leaching of marine ferromanganese precipitates: genetic implications. *Geochim. Cosmochim. Acta* **59**, 5113–5132.

Langmuir D. (1997) *Aqueous Environmental Geochemistry*. Prentice-Hall, New Jersey.

Levasseur S., Brick J.-L., and Allegre C. J. (1998) Direct measurement of femtomoles of osmium and the $^{187}Os/^{188}Os$ ratio in seawater. *Science* **282**, 272–274.

Levasseur S., Rachold V., Brick J.-L., and Allegre C. J. (2000) Osmium behaviour in estuaries: the Lena River example. *Earth Planet. Sci. Lett.* **177**, 227–235.

McDaniel D. K., Walker R. J., Hemming S. R., Horan M. F., Becker H., and Grauch R. I. (2004) Sources of osmium to modern oceans: New evidence from the $^{190}Pt-^{186}Os$ system. *Geochim. Cosmochim. Acta* **68**, 1243–1252.

Megonigal J. P., Patrick, Jr., W. H., and Faulkner S. P. (1993) Wetland identification in seasonally flooded forest soils: Soil morphology and redox dynamics. *Soil Sci. Soc. Am. J.* 57, 140–149.

Morford J. L., Martin W. R., Kalnejais L. H., Francois R., Bothne M., and Karle I. M. (2007) Insights on geochemical cycling of U, Re and Mo from seasonal sampling in Boston Harbor, Massachusetts, USA. *Geochim. Cosmochim. Acta* 71, 895–917.

O'Day P. A., Rehr J. J., Zabinsky S. J., and Brown G. E. (1994) Extended X-ray absorption fine structure (EXAFS) analysis of disorder and multiple scattering in complex crystalline solids. *J. Am. Chem. Soc.* 116, 2938–2949.

Oxburgh R. (1998) Variations in the osmium isotope composition of sea water over the past 200,000 years. *Earth Planet. Sci. Lett.* 159, 183–191.

Palmer M. R., Falkner K. K., Turekian K. K., and Calvert S. E. (1988) Sources of osmium isotopes in manganese nodules. *Geochim. Cosmochim. Acta* 52, 1197–1202.

Peucker-Ehrenbrink B., and Ravizza G. (2001) The marine osmium isotope record. *Terra Nova* 12, 205–219.

Pierson-Wickmann A.-C., Reisberg L., and France-Lanord C. (2002) Behavior of Re and Os during low-temperature alteration: Results from Himalayan soils and altered black shales. *Geochim. Cosmochim. Acta* 66, 1539–1548.

Ravizza G., and Turekian K. K. (1989) Application of the $^{187}Re/^{188}Os$ system to black shale geochronometry. *Geochim. Cosmochim. Acta* 53, 3257–3262.

Ravizza G., Turekian K. K., and Hay B. J. (1991) The geochemistry of rhenium and osmium in recent sediments from Black Sea. *Geochim. Cosmochim. Acta* 55, 3741–3752.

Ravizza G., Martin C. E., German C. R., and Thompson G. (1996) Os isotopes as tracers in seafloor hydrothermal systems; metalliferous deposits from the TAG hydrothermal area, 26 degrees N Mid-Atlantic Ridge. *Earth Planet. Sci. Lett.* 138, 105–119.

Rudolph J., Koschprreck M., and Conrad R. (1996) Oxidative and reductive microbial consumption of nitric oxide in a heathland soil. *Soil Biol. Biochem.* 28, 1389–1396.

Sakakibara N., Takahashi Y., Okumura K., Hattori K. H., Yaita T., Suzuki K., and Shimizu H. (2005) Speciation of osmium in an iron meteorite and a platinum ore specimen based on X-ray absorption fine-structure spectroscopy. *Geochem. J.* 39, 383–389.

Selby D., and Creaser R. A. (2003) Re-Os geochronology of organic-rich sediments: an evaluation of organic matter analysis. *Chem. Geol.* 200, 225–240.

Shannon R. D. (1976) Revised effective ionic radii and systematic studies of interatomic distances in halides and chalcogenides. *Acta Cryst.* A32, 751–767.

Sharma M., Papanastassiou D. A., and Wasserburg G. J. (1997) The concentration and isotopic composition of osmium in the oceans. *Geochim. Cosmochim. Acta* 61, 3287–3299.

Smoliar M. I., Walker R. J., and Morgan J. W. (1996) Re–Os ages of group IIA, IIIA IVA, and IVB iron meteorites. *Science* 271, 1099–1102.

Stern E. A. (1993) Number of relevant independent points in X-ray absorption fine-structure spectra. *Phys. Rev. B* 48, 9825–9827.

Stingl T., Mueller B., and Lutz H. D. (1992) Crystal structure refinement of osmium(II) disulfide. *Z.Kristallogr.* 202, 161–162.

Sundby B., Martinez P., and Gobeil C. (2004) Comparative geochemistry of cadmium, rhenium, uranium, and molybdenum in continental, margin sediments. *Geochim. Cosmochim. Acta* 68, 2485–2493.

Suzuki K., Qi-Lu, Shimizu H., and Masuda A. (1996) Reliable Re-Os age for molybdenite. *Geochim. Cosmochim. Acta* 57, 1625–1628.

Takahashi Y., Minai Y., Kimura T., Meguro Y., and Tominaga T. (1995) Formation of actinide(III)–humate and its influence on adsorption on kaolinite. *Mat. Res. Soc. Symp. Proc.* 353, 189–197.

Takahashi Y., Minai Y., Ambe S., Makide Y., Ambe F., and Tominaga T. (1997) Simultaneous determination of stability constants of humate complexes with various metal ions using multitracer technique. *Sci. Total Environ.* 198, 61–71.

Takahashi Y., Minai Y., and Tominaga T. (1998a) Complexation of Eu(III) with humic substances fractionated by coagulation. *Radiochim. Acta* 82, 97–102.

Takahashi Y., Kimura T., Kato Y., Minai Y., and Tominaga T. (1998b) Characterization of Eu(III) species sorbed on silica and montmorillonite by leaser-induced fluorescence spectroscopy. *Radiochim. Acta* 82, 227–232.

Takahashi Y., Minai Y., Ambe S., Makide Y., and Ambe F. (1999) Comparison of adsorption behavior of multiple inorganic ions on kaolinite and silica in the presence of humic acid using the multitracer technique. *Geochim. Cosmochim. Acta* 63, 815–836.

Tessier A., Campbell P. G. C., and Boisson M. (1979) Sequential extraction procedure for the speciation of particulate trace elements. *Anal. Chem.* 51(7), 844–851.

Tsunogai S., and Noriki S. (1983) *Kaiyo Kagaku* (ed. M. Nishimura). Sangyo Tosho, Tokyo, 82 pp.

Van Cappellen P., and Wang Y. F. (1996) Cycling of iron and manganese in surface sediments: a general theory for the coupled transport and reaction of carbon, oxygen, nitrogen, sulfur, iron, and manganese. *Am. J. Sci.* 296, 197–243.

Woodhouse O. B., Ravizza G., Falkner K. K., Statham P. J., and Peucker-Ehrenbrink B. (1999) Osmium in seawater: concentration and isotopic composition vertical profiles in the eastern Pacific Ocean. *Earth Planet. Sci. Lett.* 173, 223–233.

Zavinsky S. I., Rher J. J., Ankudinov A., Albers R. C., and Eller M. J. (1995) Multiple scattering calculations of X-ray absorption spectra. *Phys. Rev. B* 52, 2995–3009.

Associate editor: John Crusius

Development of a novel mass spectrometer equipped with an electron cyclotron resonance ion source

Masanori Kidera,[a,*] Kazuya Takahashi,[a] Shuichi Enomoto,[a] Youhei Mitsubori,[b] Akira Goto[a] and Yasushige Yano[a]

[a]Nishina Center for Accelerator-Based Science, RIKEN, 2-1 Hirosawa, Wako, Saitama 351-0198, Japan.
E-mail: Masanori Kidera (kidera@kindex.riken.jp)

[b]Faculty of Engineering Division I, Tokyo University of Science, 1-3 Kagurazaka, Shinjuku-ku, Tokyo 162-8601, Japan

The ionization efficiency of an electron cyclotron resonance ion source (ECRIS) is generally high and all elements can be fundamentally ionized by the high-temperature plasma. We focused our attention on the high potentiality of ECRIS as an ion source for mass spectrometers and attempted to customize a mass spectrometer equipped with an ECRIS. Precise measurements were performed by using an ECRIS that was specialized and customized for elemental analysis. By using the charge-state distribution and the isotope ratio, the problem of overlap, such as that observed in the spectra of isobars, could be solved without any significant improvement in the mass resolution. When the isotope anomaly (or serious mass discrimination effect) was not observed in ECR plasma, the system was found to be very effective for isotope analysis. In this paper, based on the spectrum (ion current as a function of an analyzing magnet current) results of low charged state distributions (2+, 3+, 4+, ...) of noble gases, we discuss the feasibility of an elemental analysis system employing an ECRIS, particularly for isotopic analysis. The high-performance isotopic analysis obtained from an ECRIS mass spectrometer in this study suggests that it can be widely applied to several fields of scientific study that require elemental or isotopic analyses with high sensitivity.

Keywords: ECRIS, mass spectrometer, elemental analysis, isotopic analysis, isotope anomaly

Introduction

A mass spectrometer consists of three essential components—an ion source, a mass analyzer and a detector system. These components have undergone various developments. When a mass spectrometer is used for elemental or isotopic analysis, the ion source technique is very important with regard to its ionic efficiency, stability, etc. Several types of ion source, such as the spark source, glow discharge thermal ionization source and secondary ion source, have been developed for the analyses of inorganic matter and are integrated with mass spectrometry.[1] These ion sources do not have sufficient power for measuring all types of elements and materials. Some ion sources are used only for limited elements and complex and specific chemical procedures for the

materials must be analyzed. In recent years, the inductively coupled plasma (ICP) ion source has been commonly used by combining it with various mass analyzers and detector systems. The ICP ion source of the mass spectrometer produces ions by the discharge of Ar gas under atmospheric pressure and offers the following advantages: easy sample introduction, high ionization efficiency for various elements and less interelement and matrix interferences. However, it has the disadvantage that its atmospheric pressure condition requires multiple stages of the vacuum interface system, thereby resulting in a decrease in the transmittance of ions. Another disadvantage is that it yields molecular ions easily. Recently, collision cell technology (CCT) has been developed to avoid interference from molecular ions.[1] However, this technology also leads to a decrease in the transmittance

of ions. Furthermore, the ionization efficiency of the ICP ion source for elements such as Se and As, which have relatively high electronegativity, is not the highest.

In the early 1970s, Geller proposed electron cyclotron resonance ion sources (ECRISs) for the production of highly charged ions.[2] During the past 30 years, these sources have been utilized and the highly-charged ions were enhanced. Many ECRISs are used in heavy-ion accelerators to supply stable beams of heavy ions for various accelerators and users. ECRISs produce stable and intense beams of very highly-charged positive ions from most elements of the periodic table. The ionization efficiency of commonly used ECRISs is high; for example, the ionization efficiency in a general ECR ion source is recognized to be almost 10–20%; furthermore, in the absence of a vacuum device for the plasma chamber, the ionization efficiency is reported to exceed 40% in the case of He, Ne, Ar and Kr.[3] Since 2000, we have been studying the performance of ECRISs in our accelerator facility (RILAC in RIKEN); moreover, we have observed the high performance of the ECRIS, which can work under high vacuum conditions.[4] It is expected that this ECR technology will produce an ion source that can achieve high ionization efficiency for all elements without producing molecular ions and causing interelement and matrix interferences. Further, this technique provides a breakthrough in several fields of scientific study, such as environmental, geochemical or biochemical analyses, by the successful analysis of elements that have not been analyzed with the desired sensitivity and precision by conventional techniques. Based on this feasibility study, we have developed a new mass spectrometer system equipped with an ECRIS. This system is termed as an ECRIS mass spectrometer and the ECRIS was customized for isotopic and elemental analyses. In this paper, we describe this system and introduce the primary data of the isotopic analysis.

The principle of an ECR ion source

An electron in a magnetic field exhibits cyclotronic motion. When this electron and a space electric potential (electric field), which have high frequency (frequencies in the GHz range is used as well) resonates, the electron is accelerated. This is called electron cyclotron resonance (ECR) heating. The relationship between the high frequency and the magnetic field strength at resonance is as follows:

$$Br = 0.0357 \times fc$$

where fc is the frequency [GHz] of a high frequency and Br [T] is the magnetic field strength that causes the resonance.

Further, if an electron enters a magnetic field where the slope of its magnetic strength is sharp, the electron will rebound depending on the conditions. (This phenomenon can be understood from the law of conservation of a magnetic moment.) The electron can be confined by combining the two magnetic fields. The resulting magnetic field is called

a mirror magnetic field. If Br exists in the mirror magnetic field, an electron is accelerated sequentially by ECR and becomes a high-temperature electron. ECR plasma is generated by the collision of such a high-temperature electron with a neutral atom or ion. Ions are also confined by a Coulomb force from the electrons while the electrons are confined by the mirror magnetic field. It is very important to note that due to this confinement, the electron confinement time becomes long. Since the electron has a high temperature and its (as well as that of the ion's) confinement time is long, highly-charged ions are produced easily.

R. Geller et al. have reported that the charge value, ion beam intensity and beam stability of multicharged ions can be improved rapidly by positioning the multipole magnet to obtain a confinement magnetic field in the radial direction.[2] An ECR ion source with this magnetic field distribution—the so-called minimum-B configuration—is different from an ion source that uses only a mirror magnetic field. Typically, in a cylindrical plasma chamber, the confinement of an axis direction by the mirror magnetic field and the confinement of a radial direction by the multipole magnetic field results in a longer electron confinement time and higher electron density. Hence, the minimum-B type ECR ion source has extremely stable ECR plasma and an intense beam of highly-charged ions is obtained.

Further, ECR plasma in the minimum-B type ECR ion source is generated with a very low gas pressure. For example, when high frequency is introduced in a plasma chamber maintained at a low gas pressure of 1×10^{-4} Pa by using a sample gas, ECR plasma will be produced easily. For the operation of an ECR ion source, the gas pressure and the power of high frequency (if solenoid coils are used for mirror magnetic fields, this is applicable to coil current too) are adjusted by monitoring an ion beam current so that the current reaches maximum and remains stable. An ECR ion source of this minimum-B type is used as the ion source of our ECRIS mass spectrometer.

Equipment for the ECRIS mass spectrometer

As mentioned previously, an ECR ion source with a minimum-B configuration has been commonly used as the ion source in accelerator facilities. In order to generate an intense ion beam of highly-charged ions, the ECR ion sources in these facilities are equipped with a huge magnet and a high-output, high-frequency power supply. Moreover, ions of various elements are generated from samples of various types, for example, gases, metals, oxides, organic compounds, etc. Details of the ion species and the technique of ion production in ECR ion sources can be obtained from Reference 5.

As the first step in the development of the mass spectrometer for elemental and isotopic analyses, the ECR system needed to be customized in a similar way to usual analytical instruments. It was also necessary to design
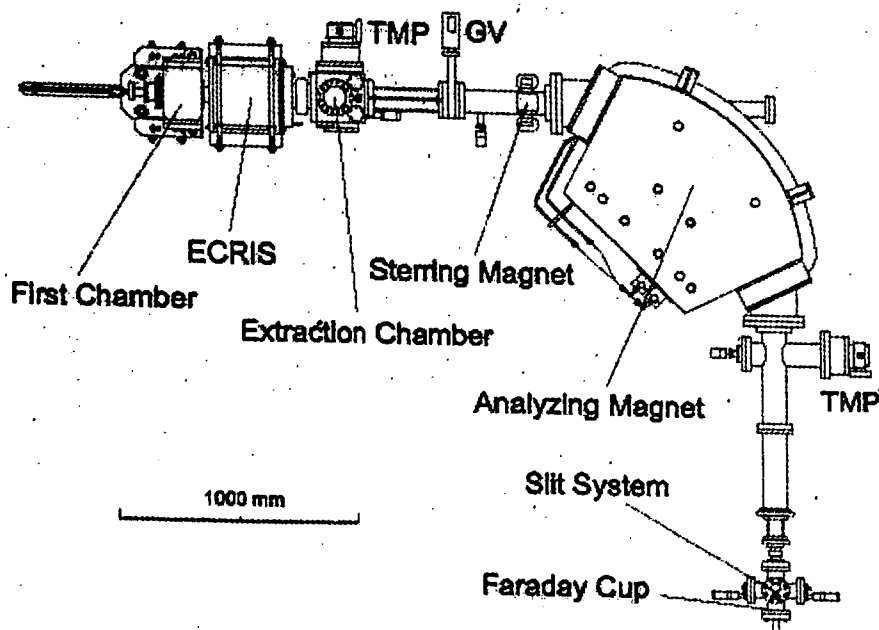
Figure 1. Schematic view of the ECRIS mass spectrometer.

the ion optics and mass analyzer systems for the ECRIS appropriately.

Figure 1 shows a schematic view of the ECRIS mass spectrometer. This system consists mainly of the ECRIS, an analyzing magnet that can focus in a vertical direction (axial focusing) by using the edge angles in the entrance and exit of the magnet and a detection system; these components are described below in detail.

Ion source (ECRIS)

The ECR ion source is the most important component that characterizes the system. The ECRIS primarily consists of the following three parts: permanent magnets for the magnetic mirror field, a high-frequency power supply and a plasma chamber. A magnetic field is produced by the permanent magnets. The permanent magnet unit was manufactured by Shin-Etsu Chemical Co., Ltd. Figure 2 shows a
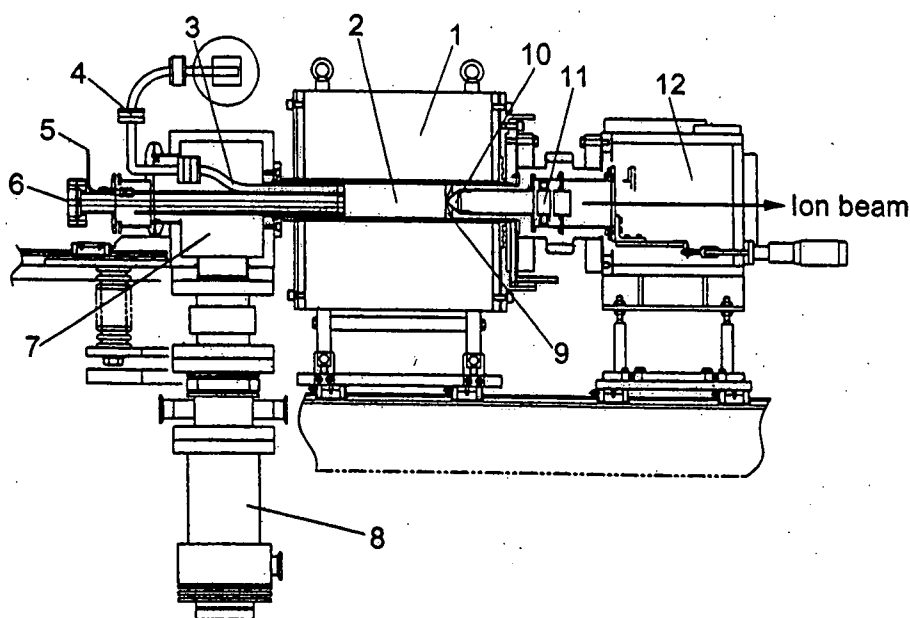

Figure 2. Cross-sectional view of the ECRIS, first chamber and extraction chamber. 1: Permanent magnets (ring magnets and hexa-pole magnet), 2: plasma chamber, 3: wave guide, 4: quartz pressure window, 5: gas feed, 6: insertion flange for sample, 7: first chamber, 8: turbomolecular pump (220 L min⁻¹), 9: plasma electrode, 10: extraction electrode, 11: Einzel lens and 12: Extraction chamber.
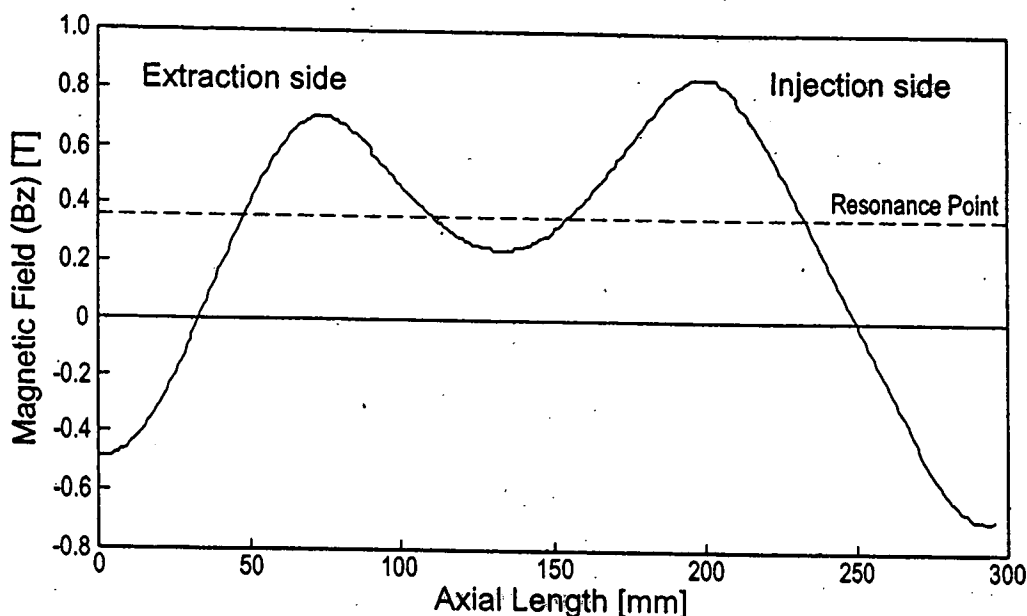
Figure 3. Distribution of magnetic field strength in the axial direction.

cross-sectional view of the ECRIS, the first chamber and the extraction chamber. The magnetic mirror field is produced by four ring magnets. A hexapole magnet is inserted into the center of the ring magnets and a magnetic field direction of the hexapole magnet is perpendicular to a magnetic field direction of the ring magnets. The magnetic field distribution in the axial direction is shown in Figure 3. When the strengths of the axial confinement magnetic field by the ring magnets and the radial confinement magnetic field by the hexapole magnet are high, the confinement of electrons is enhanced and stable plasma that contributes to the measurement precision of the mass spectrometer is generated. In order to improve the confinement of electrons by the applied magnetic field and to generate stable ECR plasma, the ECRIS has a magnetic field higher than that produced by all types of permanent magnets of typical ECRISs using high frequency of 10 GHz. As we intend to achieve a broad charge state distribution, the intensity of the magnetic field on the extraction side is slightly increased.[6] Although the total and peak ion currents tend to decrease, their values are sufficient for the analysis of the distribution.

The main specifications of the ECRIS are listed in Table 1. To prevent the demagnetization of the permanent magnets by the heat from the ECR plasma, the plasma chamber is cooled by pure water at approximately 20°C. The minimum permeance coefficient for the entire magnetic circuit is -0.275. The heatproof temperature for the permissible demagnetization range of 1% is approximately 50°C because the magnetic material of the hexapole magnet is N39UH. The first chamber, plasma chamber and extraction chamber are connected by metal seals. All the flanges of the first and extraction chambers are sealed with metal gaskets and the interiors of all the chambers are electrolytically polished. The vacuum level reaches 1×10^{-7} Pa due to sealing and polishing.

The extraction electrode, which is connected to an Einzel lens electrode, can be moved along the beam direction in the extraction chamber. The voltage of the Einzel lens was set at the value at which the ion currents in the Faraday cup were maximum. It was decided that the position of the lens should be at the position at which the peak shape of the mass spectrum improved. The space-charge effect was minimized by maintaining the value of the total beam current below a few hundred microamperes. The diameters of the holes of both

Table 1. Specifications of the ECRIS.

Mirror magnet	
Material	NdFeB
Maximum field strength	
Injection side	0.85T
Extraction side	0.70T
Minimum field strength	0.25T
Hexapole magnet	
Maximum field strength	1.48T
Chamber surface	0.85T
Length	120mm
Inner diameter	62mm
Plasma chamber	
Internal diameter	50mm
Length	160mm
High frequency	
Frequency	10GHz
Maximum power (TWTA)	650W
Wave guide	WR-75

the plasma electrode and the extraction electrode were 6 mm. The distance between the two electrodes was 21 mm. The calculated space-charge limit was almost 0.4 mA. In view of the drain current from the high-voltage power supply, the extracted total ion current was 0.18 mA or less.

In the case of our dipole magnet, the positions of the object and image focal points are at the same distances along the axis of symmetry of the magnet. The positions are 1400 mm from the entrance (or exit) of the magnet. However, with regard to the beam transport, the starting point is not clear in the case of the ECRIS. Because the spatial distribution of the extracted ions depends on the mass-to-charge ratio, the main slit behind the extraction electrode could not be used. Hence, in order to determine the location at which the resolution is the highest, the ion source component and the detection component were mounted on a slide rail, and they could, therefore, be moved linearly and smoothly.

We used a traveling-wave-tube amplifier (TWTA) manufactured by NEC Microwave Tube, Ltd. It produces a high frequency of 10 GHz and a maximum output power of 650 W. The power of the high frequency can be changed continuously. Microwaves are transmitted to the plasma chamber by a waveguide; the waveguide comprises a DC break block for isolation from the high extraction voltage and an EH tuner for high frequency matching. A vacuum is maintained in the chamber by means of a quartz pressure window developed by CPI/MPP. The flange with the pressure window is attached to the injection waveguide by using a metal O-ring. Therefore, the outgas produced by the heat by high frequency power loss in the window is minimized.

Analyzing magnet

A dipole magnet with a C-type yoke is used to analyze the multi-charged ions extracted from the ECRIS. Table 2 lists the main specifications of the analyzing magnet. For obtaining magnetic field measurements, a hall probe is installed at the center of the outer surface of the inner curve of the flight chamber. We used an Agilent 6691A power supply, which produces low ripple and noise, for the magnetic coil. The measurement accuracy of the m/z value can be improved by controlling the magnetic field

measured by the hall probe and the current monitor output of the power supply.

Detection system

Usually, the intensity of the ion current from the ECRIS is significantly higher than that of the current from other mass spectrometers. For example, ion beams of multi-charged Ar greater than 10 μA can be obtained by optimizing the high frequency power and the gas pressure. However, in this system, an injection slit cannot be used downstream of the extraction electrode because the space distribution of the ion beam extracted from an ECR ion source depends on m/z. Therefore, when a quantity and a shape of the ion beam is changed before reaching the dipole magnet by using a main slit, etc., it becomes the cause of a mass discrimination effect. Since a thin slit, etc., is not used, the ion current measured with a detection system is large in comparison with other analytical systems. Therefore, a new Faraday cup (FC) that was suitable for small and large currents with low noise was developed. The FC and a picoammeter are connected by a lead-through with double shields, triaxial cables and triaxial connectors. The FC and slit system are insulated from the beam line and trestle in order to protect them from the effect of the noise produced by the electrical discharge of the ion source and vacuum systems on the beam duct. The dark current was measured to be approximately 200 fA. There was no difference between the dark current values measured with and without the operation of the ion source. Corrector slits that can be moved in the up, down, left and right directions were installed in front of the FC.

Measurement of noble gases

By using high-purity Ar and Kr gases, each low-charged ion was measured for performance evaluation as the first step in this system. Table 3 shows the main operating parameters of the ECRIS for producing Ar and Kr ions.

Figure 4 shows the typical spectrum of the charge-state distribution of the Ar ions. The spectra (ion current as a function of the analyzing magnet current) shown in Figures

Table 2. Specifications of the analyzing magnet.

Radius of curvature	700 mm
Bending angle	90°
Pole gap	73 mm
Flight chamber gap	60.5 mm
Flight chamber width	180 mm
Edge angle	26.57°
Magnetomotive force	19200 AT
Maximum coil current	200 A
Maximum magnetic field	0.32 T

Table 3. Main parameters of the ECRIS for noble gas measurements.

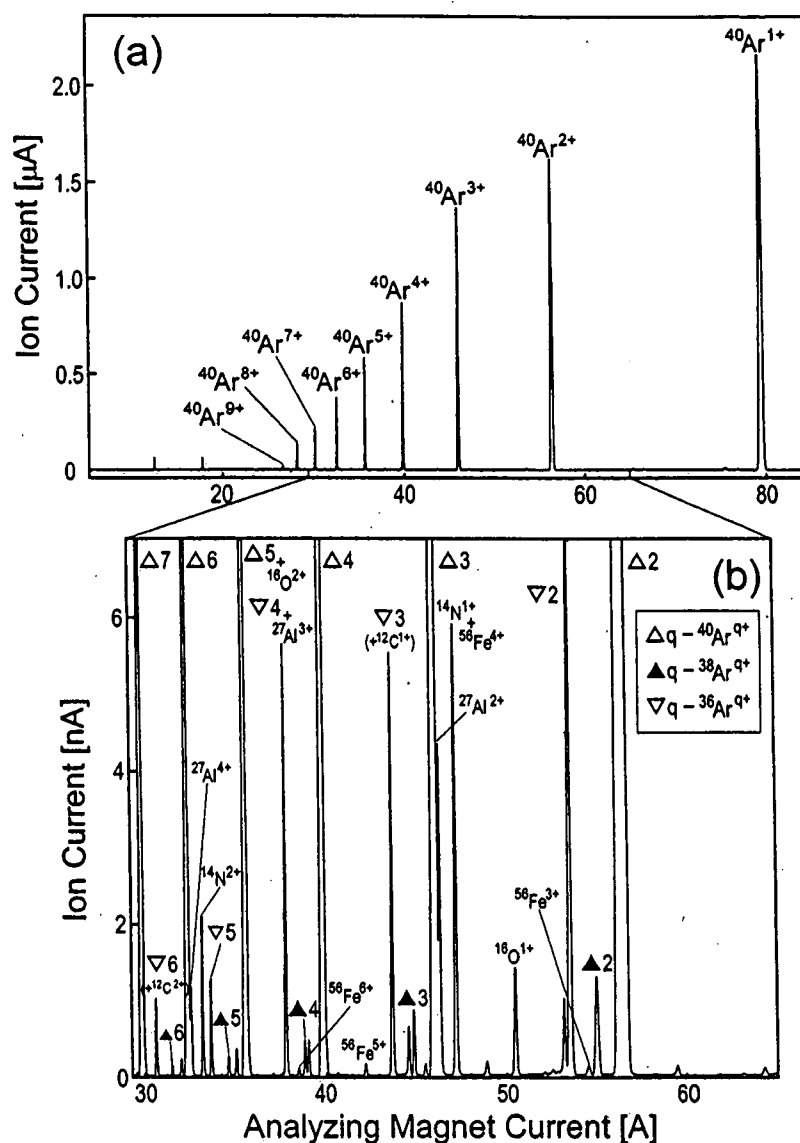|	Ar	Kr
Extraction voltage	10.00 kV	10.00 kV
Drain current	0.21 mA	0.28 mA
Einzel lens voltage	2 kV	2.6 kV
High frequency power	100 W	106 W
High frequency reflection power	3 W	12 W
Gas pressure	5.5e–5 Pa	4.0e–5 Pa

Figure 4. Ion current as a function of the analyzing magnet current. Typical spectrum of the charge-state distribution of Ar ions. Both (a) and (b) were obtained by performing the measurement once.

4(a) and 4(b) were obtained in a single measurement. Subsequently, the spectrum of the charge-state distribution of Ar was measured 10 times in 1.5 h without changing the parameters of the ion source. The duration of each measurement was approximately 5 min and the speed for scanning the magnet was approximately 0.3As^{-1}. In Table 4, the stability level of the ion current from 1+ to 8+ is shown as the standard deviation of the values obtained after performing the measurements 10 times for approximately 90 min. For the 3+ spectra of ^{40}Ar, the mass-to-charge ratio value of $^{40}\text{Ar}^{3+}$ is close to that of $^{27}\text{Al}^{2+}$. It was not possible to separate the values in the scale range of the horizontal and vertical

Table 4. Long-time (90 min) stability of Ar ion current from the ECRIS.

Charge state	1	2	3	4	5	6	7	8
Ion current[a] (nA)	1922	1638	1370	720	412	258	158	116
Stability[b] (nA)	9.8	9.3	29	18	13.3	11.5	8.8	6.8
Ratio (%)	0.51	0.57	2.2	2.5	3.3	4.6	5.6	5.9

[a]Average value obtained by measuring ten times
[b]Standard deviation

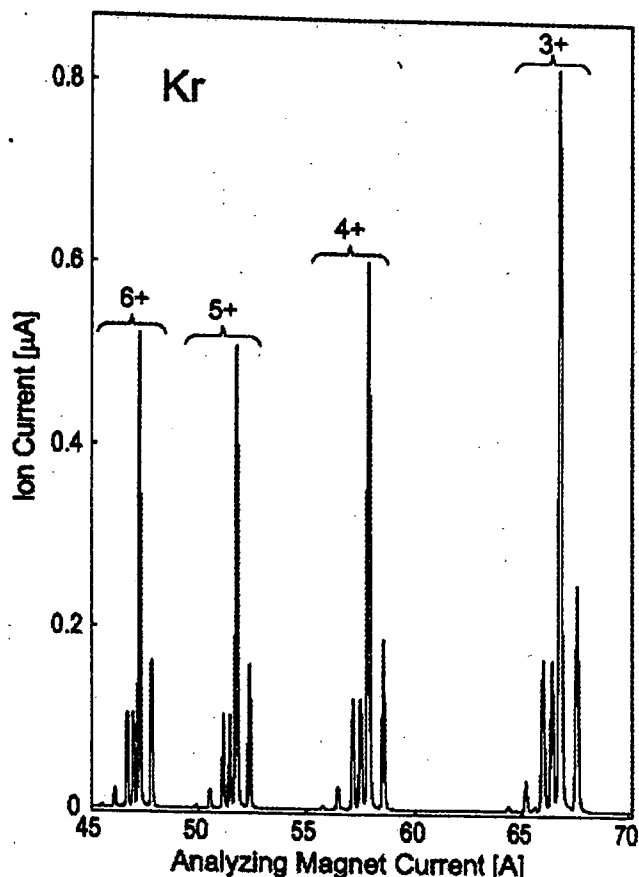**Figure 5.** Kr ion current as a function of the analyzing magnet current. Typical spectrum of the charge-state distribution of Kr ions.

high-energy electrons in the ECR plasma. Aluminum ions are generated from this cylinder. The spectrum of Fe ions was also observed in Figure 4(b) due to similar reasons. In this case, the plasma electrode was made of stainless steel 316L. It appears that the problem of overlap can be solved by changing the materials when it becomes difficult to measure the spectra. Moreover, if a clean environment is necessary for the plasma chamber, it is preferable to use a quartz tube.[7]

With the exception of ^{38}Ar, stable elements with mass numbers of 38 do not exist. In this measurement, if there is no element whose mass number is a multiple and a common divisor of 38 and the isotope of Ar does not occur, the ion currents for ^{36}Ar and ^{40}Ar are calculated from the ion current of ^{38}Ar accurately. In the charge distribution, the part of the ^{27}Al^{3+} spectrum that overlaps with the ^{36}Ar^{4+} spectrum can be determined by the subtraction of a peak height of the ^{36}Ar^{4+} spectrum. The peak height of the ^{36}Ar^{4+} spectrum is calculated from the isotope abundance of argon when there are no scientific abnormalities in the isotope ratio of argon. This indicated that the problem of overlap such as that observed in the spectra of isobars can be solved without any significant improvement in the mass resolution by using the charge state distribution and isotope ratio.

Figure 5 shows the typical spectrum of the charge-state distribution of Kr ions. By using the spectrum (Kr ion current as a function of the analyzing magnet current) obtained by a single measurement, the isotope ratio of Kr was obtained from the results of the charge states of the 3+, 4+, 5+ and 6+ spectra. This was compared with the isotope ratio in a terrestrial atmosphere[8] and is shown in Table 5. The measurement of the spectrum was carried out once. This spectrum was recorded with an X–Y pen recorder. The standard deviation for measuring the isotope of each charge number with a vernier micrometer was very small. The error margin in the measurement accuracy (+/–0.05 mm) of the vernier micrometer was larger than the standard deviation. The measurement by the vernier micrometer was performed once. With regard to the error margin given in Table 5, the error in the

axis of Figure 4(a). Hence, it was considered that these values changed due to the overlapping of the two spectra. The two spectra were separated, as shown in Figure 4(b), by doubling the scale of the spectra shown in Figure 4(a). The inner cylinder was made of pure Al in order to protect the plasma chamber from being heated up by the spattering of

Table 5. Isotopic ratio of Kr in comparison with that in the terrestrial atmosphere.

	^{78}Kr/^{84}Kr	^{80}Kr/^{84}Kr	^{82}Kr/^{84}Kr	^{83}Kr/^{84}Kr	^{86}Kr/^{84}Kr
ECRIS mass spectrometer +/–	6.1e–3 0.4e–3	0.0397 0.0004	0.202 0.001	0.200 0.001	0.308 0.001
Terrestrial atmosphere[a] +/–	6.10e–3 0.03e–3	0.0396 0.0002	0.2022 0.0005	0.2016 0.0005	0.3055 0.0007

[a]See Reference 8. All ratios were normalized by ^{84}Kr. The error margin was simply calculated from the percent ratio of each error margin.

Table 6. Ingredients of the standard gas chosen from noble gases.

Ingredient	He	Ne	Ar	Kr	Xe
Purity	99.9995%	99.99%	99.99%	99.99%	99.99%
Amount	Balance	101 ppm	101 ppm	102 ppm	102 ppm

Table 7. Evaluation of the precision of isotopic analysis of noble gas compounds. Upper subscript "m" represents atomic mass numbers to the line. "M/z" is mass-to-charge ratio.

M/z	124	126	128	129	130	131	132	136			
^{m}Xe$^+$/^{134}Xe$^+$	124	126	128	129	130	131	132	136			
	0.00910	0.00875	0.188	2.540	0.3912	2.049	2.575	0.8471			
err.(+/−)	0.00005	0.00004	0.003	0.008	0.0032	0.007	0.008	0.0039			
M/z	78	80	82	84	86						
^{m}Kr$^+$/^{83}Kr$^+$	78	80	82	84	86						
	0.034	0.252	1.013	4.997	1.477						
err.(+/−)	0.001	0.002	0.007	0.025	0.009						

M/z	39	40	41	41.3	42	42.6	43	43.3	43.6	44	45.3
^{m}Kr^{2+}/^{83}Kr^{2+}	78	80	82		84		86				
	0.078	24.7	1.11		4.86		1.56				
err.(+/−)	—	—	0.07		0.02		0.01				
^{m}Xe^{3+}/^{134}Xe^{3+}				124	126	128	129	130	131	132	136
				—	—	0.16	2.603	0.370	2.047	3.364	0.8309
err.(+/−)				—	—	0.01	0.002	0.005	0.013	—	0.0076

Terrestrial atmosphere

M/z	124	126	128	129	130	131	132	136			
^{m}Xe/^{134}Xe[a]	124	126	128	129	130	131	132	136			
	0.009096	0.008477	0.1834	2.534	0.3896	2.035	2.577	0.8500			
err. (+/−)	0.000055	0.000055	0.0007	0.006	0.0011		0.005	0.0023			
^{m}Kr/^{83}Kr[b]	78	80	82	84	86						
	0.0303	0.196	1.003	4.960	1.515						
err.(+/−)	0.0001	0.001	0.002	0.011	0.003						

[a]See Reference 11. All ratios were normalized by ^{134}Xe. The error margin was simply calculated from the percent ratio of each error margin.

[b]See Reference 8. All ratios were normalized by ^{83}Kr. The error margin was simply calculated from the percent ratio of each error margin.

measurements performed with the vernier micrometer was used. The results obtained by using the charge-state distribution in the measurement performed once with high precision are in good agreement with the reference data. The error limits are estimated from the precision of the measurements of the peak height with a vernier micrometer. It should be noted that the above-mentioned results are obtained without any regular alignment of the ion source, the FC systems and beam optics.

From our preliminary data, we have not identified any apparent isotope effects or fractionations that depend on the mass. Kawai et al. have reported such isotope effects (mass discrimination effect) for nitrogen in an ECRIS.[9] They have explained the isotope anomaly (mass discrimination) based on the ion Landau damping due to the influence of low-frequency noise. In relation to the ion Landau damping, the possibility of mass discrimination due to the effect of gas mixing might have to be considered. The gas mixing method has been researched and used widely in the ECRISs of many accelerator facilities where an intense beam of highly-charged ions is required. The beam intensities of the highly-charged
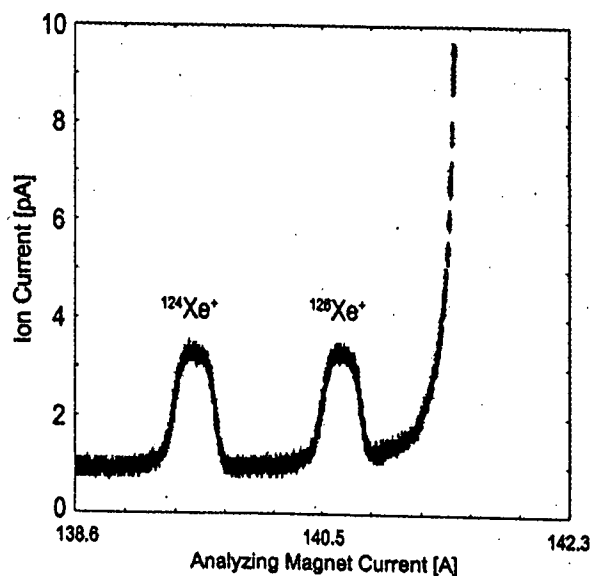

Figure 6. Spectrum of 1+charge state of ^{124}Xe and ^{126}Xe; the relative abundances of these elements are 0.10% and 0.09%, respectively.

ions of Ar were (or were not) altered by mixing gases such as H, He, ^{14,15}N and ^{16,18}O. It is thought that this effect influences the charge-state distribution through ion cooling.[10] Depending on the selected gas, the influence of ion cooling might alter the isotope ratio of a low-charge state. This influence on the isotope ratio of low-charge states (2+, 3+, 4+, ...) has not been systematically examined in the mixing of metal elements and various gases. In our isotope measurements of pure Kr, a systematic isotope anomaly (mass discrimination) was not observed within the measurement precision. In ECR plasma, a careful observation of the isotope anomaly (mass discrimination) in the low-charge state should be conducted in the future.

Preliminary measurements with a standard gas

For the demonstration of elemental analysis employing low charge-state distribution, a standard gas chosen from the noble gases was measured by this system. The ingredients of the standard gas are listed in Table 6. Eight spectra, which appropriately changed the range of the mass-to-charge ratio values and the current meter, were obtained. The analytical values in Table 7 were derived from the results of the single measurement of peak heights in the above-mentioned eight spectra with the vernier micrometer. Figure 6 shows the spectra of ^{124}Xe$^+$ and ^{126}Xe$^+$. The provisional sensitivity in this preliminary measurement was 0.1 ppm as observed in Figure 6. In the measurement employing this standard gas, Kr$^+$ and Xe$^+$ do not have the same mass numbers as those of the other elements. Therefore, Kr$^+$ and Xe$^+$ in Table 7 are the values pertaining only to Kr and Xe, respectively. It could be inferred that there was no serious isotope anomaly (or mass discrimination) in Kr and Xe from these values. Because it is the analytical value from only one charge state, the error margin is large in comparison with that of Kr in Table 5. The peaks of ^{126,129}Xe^{3+} overlapped with the peaks of ^{84,86}Kr^{2+}, respectively. The isotope ratio of ^{129}Xe^{3+} was calculated by using the isotope abundance of ^{86}Kr^{2+}. On the contrary, the isotope ratios of ^{84,86}Kr^{2+} in the table were calculated by using the isotope abundances of ^{126,129}Xe^{3+}, respectively. Accurate isotope ratios of ^{84,86}Kr^{2+} and ^{129}Xe^{3+} were derived by this method. In the isotope ratio of ^{80}Kr^{2+}, ^{40}Ar$^+$ was mainly included. Ultratrace elements of Ag, Cd and Sn were observed in this experiment. The presence of these elements is thought to be due to the use of silver brazing filler metals in order to connect the square flanges of the waveguide, which is used to introduce the high frequency into the system. The isotope ratios of ^{78}Kr^{2+} and Ar could not be calculated with good precision because of this contamination. If these contaminations pose acute problems, the problems are solved by using a waveguide that does not use silver brazing. Further, in the isotope ratio of ^{132}Xe^{3+}, CO_2 was possibly included. Concerning the origin of CO_2, the background of the system and/or the contaminations in the standard gas were enumerated. However, in both cases, the amounts obtained were inconsistent. Hence, it will be necessary to investigate the origin of CO_2 in detail in the future.

The measurement of each of the above-mentioned spectra and the analysis with the vernier micrometer was performed only once. If measurements are carried out for the flat top of the peaks and a multi-collector and a data-taking system with statistical measurements are employed, it is clear that the measurement precision and the detection sensitivity can be significantly improved.

Consideration of sample form

In this measurement, a gaseous sample was introduced into the ECRIS. The gaseous sample is suitable for the ECRIS because it can control a very small amount of gas in the plasma chamber. In the case of solid samples, particularly in metal ion production, many production techniques such as the insertion method, metal ions from volatile compounds (MIVOC) method, micro-oven method, IH oven method and the spatter method have been developed and improved by many researchers in the field of ECRIS research.[5] However, the direct ionization of a liquid sample in the ECRIS has not been investigated extensively because it is difficult to maintain a steady supply into the high vacuum chamber. Usually, ECR plasma is generated in the vacuum range from 10^{-2} to 10^{-5} Pa. In this range, it is possible to control the stable feeding and the evaporation of gas and solid samples. Liquid samples are primarily used in the field of elemental analysis. Currently, we are developing a method for the introduction of a liquid sample into the ECRIS.

Conclusions

Precise measurements are performed on Ar and Kr gases by using an ECRIS that has been customized for elemental analysis. The measurement results of Ar indicate that long-time stable ionization can be achieved without operating the ECRIS. It means that ECR plasma is stable for a long time, without readjusting the ion source parameter. The measurement results of Kr reveal that the elemental analysis system equipped with this ion source can be successfully used for isotope analysis. In this measurement, a systematic isotope anomaly (or mass discrimination) is not observed. Furthermore, in the measurement of the noble gas compound, we indicated the possibility of isotopic analysis by using the ECR ion source and a low-charge state. In the future, the isotope anomaly (mass discrimination effect) will be investigated in detail by using this analysis system, which can perform precise measurements. In order to increase the profitability of this system, it is crucial to develop a method for introducing a liquid sample in the ECRIS. The ECRIS can be expected to show a high performance for most of the elements of the periodic table and to be applicable to several scientific

fields such as environmental, material, geochemical and bioanalytical chemistry that require isotopic and elemental analyses.

Acknowledgments

References

1. F. Adams, R. Gijbels and R. Van Grieken, *Inorganic Mass Spectrometry*. Wiley Interscience, New York, USA and references therein (1988).

2. R. Geller, *Electron Cyclotron Resonance Ion Sources and ECR Plasmas*. IOP, Bristol, UK and references therein (1996).

3. P. Jardin, C. Barue, C. Canet, M. Dupuis, J.L. Flambard, G. Gaubert, N. Lecesne, P. Leherissier, F. Lemagnen, R. Leroy, J.-Y. Pacquet, F. Pellemoine, J.-P. Rataud, M.G. Saint Laurent and A.C.C. Villari, "Mono 1000: A simple and efficient 2.45 GHz electron cyclotron resonance ion source using a new magnetic structure concept", *Rev. Sci. Instrum.* **73**, 789 (2002). doi: 10.1063/1.1430869

4. M. Kidera, T. Nakagawa, K. Takahashi, S. Enomoto, R. Hirunuma, K. Igarashi, M. Fujimaki, E. Ikezawa, O. Kamigaito, M. Kase and Y. Yano, "Novel Technique for Trace Element Analysis using the ECRIS and Heavy Ion Linear Accelerator (ECRIS-AMS)", *AIP Conference Proceedings of the 16th International Workshop on ECR Ion Sources* **749**, 85 (2005). doi: 10.1063/1.1893372

5. Conference Proceedings of the *16th International Workshop on ECR Ion Sources AIP*, CA, USA **749**, and references therein (2005).

6. M. Imanaka, T. Kurita, M. Tukada, T. Nakagawa, M. Kidera, and S.M. Lee, "Effect of Magnetic Field Strength on Beam Intensity of Highly Charged Xe Ions from Liquid-He-Free Superconducting Electron Cyclotron Resonance Ion Source", *Japan. J. Appl. Phys.* **41**, 3926 (2002). doi: 10.1143/JJAP.41.3926

7. Ph. Collon, M. Bichler, J. Caggiano, L. DeWayne Cecil, Y. El Masri, R. Golser, C. L. Jiang, A. Heinz, D. Henderson, W. Kutschera, B.E. Lehmann, P. Leleux, H.H. Loosli, R. C. Pardo, M. Paul, K.E. Rehm, P. Schlosser, R.H. Scott, W.M. Smethie, Jr. and R. Vondrasek, "Development of an AMS method to study oceanic circulation characteristics using cosmogenic ^{39}Ar", *Nucl. Instrum. Methods* **B223**, 428 (2004). doi: 10.1016/j.nimb.2004.04.081

8. S. Niedermann and O. Eugster, "Noble gases in lunar anorthositic rocks 60018 and 65315: Acquisition of terrestrial krypton and xenon indicating an irreversible adsorption process", *Geochim. Cosmochim. Acta* **56**, 493 (1992). doi: 10.1016/0016-7037(92)90147-B

9. Y. Kawai, D. Meyer, A. Nadzeyka and K. Wiesemann, "Isotope effects in an electron cyclotron resonance ion source in mixtures of ^{15}N/^{14}N", *Plasma Sources Sci. Tech.* **10**, 451 (2001). doi: 10.1088/0963-0252/10/3/309

10. A.G. Drentje, A. Girard, D. Hitz and G. Melin, "Role of low charge state ions in electron cyclotron resonance ion source plasmas", *Rev. Sci. Instrum.* **71**, 623 (2000). doi: 10.1063/1.1150332

11. F.A. Podosek, J.C. Huneke, D.S. Burnett and G.J. Wasserburg, "Isotopic composition of xenon and krypton in the lunar soil and in the solar wind", *Earth Planet. Sci. Lett.* **10**, 199 (1971). doi: 10.1016/0012-821X(71)90008-2

Letter: New fragment ion production method using super cold electrons in electron cyclotron resonance plasma

Masanori Kidera, Kazuya Takahashi, Shuichi Enomoto, Akira Goto and Yasushige Yano

Nishina Center for Accelerator-Based Science, RIKEN, 2-1 Hirosawa, Wako, Saitama 351-0198, Japan. E-mail: kidera@kindex.riken.jp

We examined the fragmentation and ionization of molecules by low-temperature electrons generated by electron cyclotron resonance (ECR) plasma. We examined several types of metallocene compounds comprising a metal and 1,3-cyclopentadienes as ligands. We performed analyses using an ECR ion source (ECRIS) mass spectrometer. Consequently, we succeeded in ionizing fragments of an organometallic compound by adjusting the input power of the microwave introducing a super high-frequency plasma. Moreover, we succeeded in dynamically generating a significant quantity of fragment ions by continuously varying the input power. Information on the structure of a molecule may be acquired from this operation. Moreover, a molecule that could not be easily ionized thus far may now be ionizable when soft ionization is performed with this technique.

Introduction

Devices that employ the electron cyclotron resonance (ECR) phenomenon are widely used in applications such as etching by plasma chemical vapor deposition (CVD), ion sputtering of devices and research on nuclear fusion reactors. An ECR ion source, particularly ECR ion sources used in heavy ion accelerators, is an ECR plasma device in which the plasma is confined in a characteristic magnetic field. Such ECR ion sources are of the minimum-B configuration developed by R. Geller *et al.* in 1960.[1] Since such ion sources confine electrons very well, the electron temperature can easily be increased and they can be used to supply an intense beam of highly-charged ions. On the other hand, since the electron confinement is very strong, even if the high-frequency input power for plasma production is quite low, the plasma is stably produced. We investigated this state in greater detail using our ion source[2] and the ECR plasma was generated by an input radio frequency (RF) power very as low as 55 mW.

In the case of electron ionization (EI), thermal electrons are used as the electron source and it is difficult to control low-temperature electrons with a high electron density;

in contrast, the electron temperature can be controlled by varying the RF power in ECR ion sources. Moreover, due to the effect of electron confinement, it is expected that the collision rate will be greater than that in the EI method. This implies that the ionization efficiency will be good. The ionization efficiency is reported to exceed 40% in the case of He, Ne and Kr.[3] We have focused on the above-mentioned characteristics of ECR ion sources and examined the ionization with fragmentation for several metallocene compounds.

Ionization of molecules by using ECR plasma

First, we introduced nickelocene into the ECR plasma to examine the ionization of its molecules and to check the plasma status. When the plasma was not generated (i.e. the RF power is OFF), no ions were detected only by supplying an extraction voltage and feeding the evaporation gas of the organometallic compound. Next, when the RF power was increased gradually and it reached approximately 0.65 W, the plasma was generated. After the plasma was produced, even if the RF power was decreased gradually, the plasma was stably preserved. Figure 1 shows the variation in the